Transportation Research Part B 205 (2026) 103405

Contents lists available at ScienceDirect

Transportation Research Part B

journal homepage: www.elsevier.com/locate/trb

Capturing stochastic variabilities in pedestrian flows: A dynamic continuum modeling approach

Zepeng Liu [a], Haoyang Liang [b,*], S. C. Wong [c,*], Chi-Wang Shu [d], Mengping Zhang [e]

[a] School of Mathematics, Hefei University of Technology, 230009, Hefei, Anhui, China
[b] Ministry of Education, Key Laboratory of Road and Traffic Engineering, Tongji University, Shanghai, China
[c] Department of Civil Engineering, The University of Hong Kong, Hong Kong, China
[d] Division of Applied Mathematics, Brown University, 02912, Providence, RI, USA
[e] School of Mathematical Sciences, University of Science and Technology of China, 230026, Hefei, Anhui, China

ARTICLE INFO

Keywords:
Pedestrian dynamics
Stochastic model
Stochastic partial differential equations
Monte Carlo method
Quasi Monte Carlo method

ABSTRACT

Stochastic phenomena are commonly observed in pedestrian flow. However, the existing models for pedestrian dynamics rely on averaged inputs and yield deterministic outputs only, and thereby fail to capture the stochastic variabilities inherent in pedestrian dynamics. This study builds upon Hughes' dynamic continuum model to develop mathematical models for stochastic pedestrian dynamics that explicitly consider two types of stochastic characteristics: demand stochasticity and behavioral stochasticity. The proposed system, represented as a set of time-dependent stochastic partial differential equations, is solved using a combination of the Monte Carlo (MC) method or Quasi Monte Carlo (QMC) method and efficient numerical schemes, such as a fifth-order weighted essentially non-oscillatory finite difference scheme and the fast sweeping method. Benchmarking scenarios are designed and simulated, and the numerical results demonstrate the convergence and computational performance of the MC and QMC methods. The advantage of stochastic modeling is evident given the significant differences between the averaged stochastic outputs and deterministic outputs, attributable to the strength of stochasticity and extent of stochastic dimensions. Moreover, based on stochastic data inputs, the proposed stochastic models and numerical solutions can clarify the probabilistic distributions of key indicators, such as density, which are valuable for the design and improvement of pedestrian facilities.

1. Introduction

Pedestrian flow must be accurately modeled to investigate pedestrian dynamics. Over the past two decades, macroscopic models based on the continuum theory of mass (Hughes, 2002) and momentum (Jiang et al., 2010) have garnered significant research interest due to their computational efficiency and analytical capabilities for key variables and parameters (Jiang et al. 2011; Cao et al. 2015; Liang et al. 2021). By transforming dynamic problems into sets of time-dependent partial differential equations (PDEs), these mathematical models can capture and simulate collective movement patterns in various scenarios, such as those involving congestion (Huang et al., 2009), lane formation (Yuan et al., 2020), and density waves (Liang et al., 2021). However, these models rely on

* Corresponding authors.
E-mail addresses: lzp0375@hfut.edu.cn (Z. Liu), lianghy@connect.hku.hk (H. Liang), hhecwsc@hku.hk (S.C. Wong), chi-wang_shu@brown.edu (C.-W. Shu), mpzhang@ustc.edu.cn (M. Zhang).

https://doi.org/10.1016/j.trb.2026.103405
Received 2 July 2023; Accepted 19 January 2026
Available online 27 January 2026

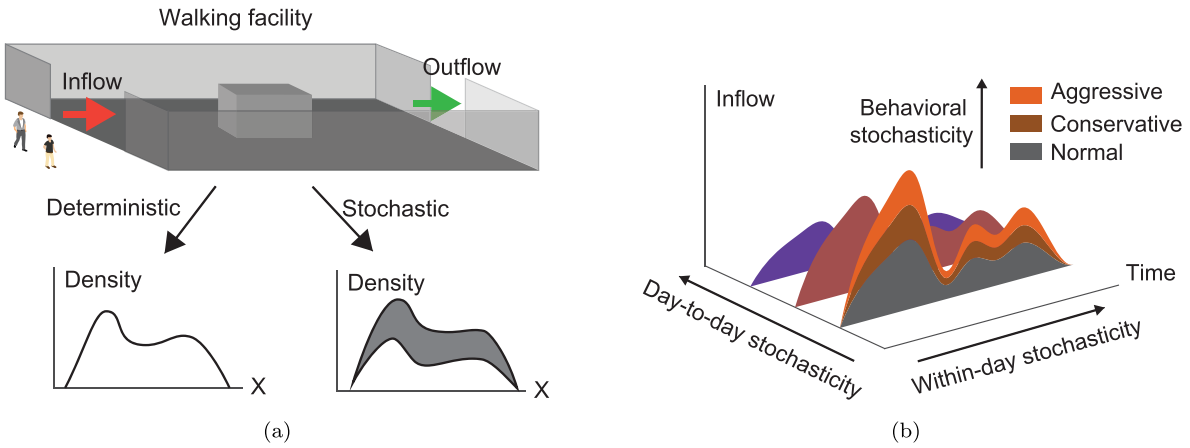

Fig. 1. Capturing stochasticity in pedestrian modeling.

averaged inputs and thus tend to ignore the inherent stochasticity in real-world situations, such as demand stochasticity, thereby providing an incomplete understanding of state evolution. For instance, in a walking facility, as shown in Fig. 1, deterministic models can only produce density estimates using averaged inputs for the demand and behavioral parameters, ignoring the probabilistic nature of demand and behavior. This limitation diminishes the effectiveness of simulation-based predictions when integrated into data-driven approaches, such as the probabilistic estimation of travel demand by Hänseler et al. (2017). Moreover, a walking facility design based solely on a deterministic model with averaged values is prone to failure approximately half of the time, while simply increasing the remaining capacity could lead to a waste of resources. Therefore, it is crucial to develop pedestrian models that explicitly consider the stochasticity in pedestrian dynamics.

Stochasticity is a common feature of pedestrian flow (Sumalee et al. 2011a; Ezzati Amini et al. 2019) and can be classified into demand stochasticity and behavioral stochasticity, as illustrated in Fig. 1. First, traffic demand is a complex phenomenon influenced by various factors, such as weather conditions and economic activities. For example, more people are observed entering underground stations on rainy days (Sumalee et al., 2011a), resulting in a more complex inflow compared with that on normal days. This phenomenon is referred to as day-to-day stochasticity. Similarly, within-day stochasticity refers to unpredictable variations in the inflow within the observation period. Second, behavioral stochasticity refers to the variability in pedestrians' behavior, typically characterized by random fluctuations in factors such as emotions, walking styles, and decision-making. For example, pedestrians may exhibit aggressive, normal, or conservative walking behaviors, with each behavior corresponding to different speeds, personal space preferences, and reactions to surrounding conditions. To date, only a limited number of macroscopic models for pedestrians have effectively incorporated these stochastic elements.

In the field of vehicular traffic, stochastic phenomena have been extensively studied. Sumalee et al. (2011b) and Zhong et al. (2013) explicitly considered demand and supply uncertainties in the stochastic cell transmission model to calculate the probabilistic density. In addition to addressing stochastic parameters from external sources, researchers have attempted to quantify the impact of stochasticity arising from inherent characteristics by randomizing the relationships among flow, density and velocity. For example, Li et al. (2012) incorporated a stochastic fundamental diagram into their modified Lighthill-Whitham-Richards (LWR) model, and Jabari et al. (2014) derived the stochastic relationship between macroscopic variables based on Newell's simplified car-following model. Fan et al. (2023, 2024) investigated the stochasticity of the LWR model arising from driver heterogeneity by randomizing speed-density relationships. In addition, Brilon et al. (2005) introduced a realistic concept of stochastic capacities, and Kerner and Klenov (2006) and Kesting et al. (2010) then implemented it to identify the characteristics of traffic flow breakdown and occurrence conditions. Recent research (Ngoduy 2021; Bouadi et al. 2022) has also focused on the connection between stochasticity and traffic instability and has attempted to capture it using higher-order continuum models.

Although a well-established framework exists for addressing stochastic phenomena in vehicular traffic, the number of stochastic models developed for pedestrian flow is limited. The relevant studies have primarily focused on incorporating stochastic inputs into microscopic models. For instance, Tordeux and Schadschneider (2016) introduced stochastic noise into optimal velocity models for pedestrians, resulting in the emergence of stop-and-go waves. Ramírez et al. (2019) implemented a cellular automaton model parameterizing social, cultural and psychological factors as sources of randomness to capture the complex random interactions of pedestrians. However, the physical interpretations of these stochastic inputs remain uncertain and require further investigation. Recent research has adopted an alternative stochastic method-game theory to advance the modeling of pedestrian flow. Specifically, mean-field game theory has been applied to study crowd motion, congestion, and evacuation dynamics (Dogbé 2010; Lachapelle and Wolfram 2011; Burger et al., 2013; Djehiche et al., 2017). Further research has deepened the connections between game-theoretic models and classical continuum models (Barreiro-Gomez and Masmoudi 2023; Ghattassi and Masmoudi 2025). However, the integration of stochasticity into macroscopic models remains an under-explored area of research, with relatively few studies dedicated to this approach.

Therefore, this study proposes a novel framework for evaluating pedestrian dynamics that explicitly considers both demand stochasticity and behavioral stochasticity. The stochastic problems are formulated as sets of partial differential equations (PDEs) with stochastic inputs. The most commonly used solution algorithm for these stochastic problems combines the classic Monte Carlo (MC) method with high-order numerical schemes for deterministic PDEs to ensure robustness. This solution framework has been successfully applied to various stochastic vehicular problems (Parry and Hazelton 2013; Sayegh et al. 2018; Fan et al. 2023). Additionally, the Quasi Monte Carlo (QMC) method has gained popularity in recent years for solving stochastic problems due to its accelerated convergence (Caflisch, 1998). The advantage of QMC lies in its ability to improve computational efficiency through quasi-random sequences without altering problem formulations, making it a robust solution framework for stochastic problems. Both the MC and QMC methods are investigated and compared in the numerical solutions for PDEs in this study.

The remainder of this paper is organized as follows. Section 2 revisits Hughes' continuum model and describes the incorporation of two critical aspects of pedestrian dynamics, demand stochasticity and behavioral stochasticity, into this model. By introducing random variables into the original PDEs, both problems are formulated as separate sets of PDEs with stochastic inputs. These equation sets are proven to be solvable using a combination of either the MC or QMC method and efficient numerical schemes, as discussed in Section 3. In the numerical examples presented in Section 4, benchmarking scenarios with stochastic inputs are designed and simulated to demonstrate the effectiveness of the stochastic model and efficiency of the numerical solvers. Section 5 presents some concluding remarks.

2. Hughes' continuum model

This section revisits the deterministic continuum model proposed by Hughes (2002), which describes the fundamental diagram and route strategy within a continuum framework. Two types of stochastic problems, demand stochasticity and behavioral stochasticity, are then explicitly considered by introducing random variables into the original PDE set.

2.1. Deterministic model

Following the framework proposed by Hughes (2002) and Huang et al. (2009), a two-dimensional walking facility is considered as a continuum within a domain Ω. The model can be characterized by the following differential equations:

$$\rho_t(x,y,t) + \nabla \cdot \boldsymbol{f}(x,y,t) = 0, \qquad \forall (x,y) \in \Omega, \quad t \in T, \tag{1a}$$

$$c(x,y,t)\frac{\boldsymbol{f}(x,y,t)}{\|\boldsymbol{f}(x,y,t)\|} = -\nabla\phi(x,y,t), \qquad \forall (x,y) \in \Omega, \quad t \in T, \tag{1b}$$

$$\|\nabla\phi(x,y,t)\| = c(x,y,t), \qquad \forall (x,y) \in \Omega, \quad t \in T. \tag{1c}$$

Here, Γ is the boundary of Ω and is expressed as $\Gamma = \Gamma_o \cup \Gamma_h \cup \Gamma_d$, where Γ_o, Γ_h and Γ_d are the entrance, wall and exit of the walking facility, respectively. T is the time horizon. $\rho(x,y,t)$ is a time-varying function that represents the pedestrian density. $\boldsymbol{f}(x,y,t) = (f_1(x,y,t), f_2(x,y,t))$ represents the flow vector, where $f_1(x,y,t)$ and $f_2(x,y,t)$ denote the flow flux in the x- and y-directions, respectively. The density and flow of pedestrians follow the physical principle of mass conservation, as expressed in Eq. (1a). The flow intensity $\|\boldsymbol{f}(x,y,t)\|$, which is determined as the norm of the pedestrian flow, is equal to the product of speed and density, i.e.

$$\|\boldsymbol{f}(x,y,t)\| = \rho(x,y,t)v(x,y,t). \tag{2}$$

Similar to the LWR model in vehicular flow, the pedestrian fundamental diagram (PFD) is also assumed to have a functional relationship that can describe the average behavior of pedestrians. Several forms of the PFD have been developed, such as Greenshields' model (Huang et al., 2009) and Drake's model (Wong et al., 2010). A recent study validated that Newell's model (Newell, 1961) can flexibly fit observed speed-density diagrams (Parisi et al., 2021), and thus the model is applied in this study. In this framework, the local walking speed $v(x,y,t)$ depends on the density at location (x,y) and is determined as

$$v(x,y,t) = U(\rho(x,y,t)) = u_f\left\{1 - \exp\left[\frac{C_0}{u_f}\left(1 - \frac{\rho_{\max}}{\rho}\right)\right]\right\}, \tag{3}$$

where u_f is the averaged free-flow walking speed of pedestrians, and C_0 is a parameter governing the backward wave speed at maximum density $\rho_{\max}$.

The reactive user-equilibrium model that describes the route strategy of pedestrians is another important assumption in Hughes' continuum model. Generally, pedestrians are assumed to move along the path that minimizes their (estimated) travel time while tempering this behavior to avoid extremely high densities. Therefore, a static eikonal equation is derived, as shown in (1c), where $c(x,y,t)$ is the local cost per unit distance of movement at location (x,y) and time t. This cost depends on the walking speed and pedestrian density, defined as

$$c(x,y,t) = C(\rho(x,y,t)) = \frac{1}{U(\rho)} + G(\rho). \tag{4}$$

The first term on the right-hand side represents the local cost associated with the (estimated) travel time. The second term represents the level of discomfort, which is assumed to be a monotonically increasing function with density and is denoted as $G(\rho)$.

$\phi(x,y,t)$ is the instantaneous walking time potential from location (x,y) to Γ_d, where $\phi = 0$. This potential function measures the total walking time along the instantaneous shortest path between location (x,y) and the destination, based on the traffic condition

at a given moment t. According to Hughes (2002) and Huang et al. (2009), Eq. (1b) ensures that a pedestrian at location $(x, y) \in \Omega$ selects a route that minimizes their individual travel cost to the destination, considering the instantaneous travel cost information.

The system is subject to the following initial boundary conditions:

$$\boldsymbol{f}(x,y,t)\cdot\boldsymbol{n}(x,y)=q(x,y,t), \qquad \forall(x,y)\in\Gamma_o,\quad t\in T, \tag{5a}$$

$$\rho(x,y,0)=\rho^0(x,y), \qquad \forall(x,y)\in\Omega, \tag{5b}$$

$$\phi(x,y,t)=0, \qquad \forall(x,y)\in\Gamma_d,\quad t\in T, \tag{5c}$$

where $\boldsymbol{n}(x, y)$ is a unit outer normal vector pointing out of the domain boundary, and $\rho^0(x, y)$ is the initial pedestrian density. The time-varying pedestrian demand on the origin segments, $q(x, y, t)$, indicates the number of pedestrians crossing a unit width of the original segment.

2.2. Stochastic model

Based on the deterministic model, random variables and boundary conditions are introduced to represent the demand stochasticity and behavioral stochasticity, which are described as Problem A and Problem B, respectively.

2.2.1. Problem A: Demand stochasticity

In the context of demand stochasticity, the magnitude of inflow, which represents the boundary condition at the inflow region, is considered to follow a probabilistic distribution. Then, the following equations can be derived based on Eq. (1):

$$\rho_t(x,y,t,\omega)+\nabla\cdot\boldsymbol{f}(x,y,t,\omega)=0, \qquad \forall(x,y)\in\Omega,\quad t\in T,\quad \omega\in\Theta, \tag{6a}$$

$$c(x,y,t,\omega)\frac{\boldsymbol{f}(x,y,t,\omega)}{\|\boldsymbol{f}(x,y,t,\omega)\|}=-\nabla\phi(x,y,t,\omega), \qquad \forall(x,y)\in\Omega,\quad t\in T,\quad \omega\in\Theta, \tag{6b}$$

$$\|\nabla\phi(x,y,t,\omega)\|=c(x,y,t,\omega), \qquad \forall(x,y)\in\Omega,\quad t\in T,\quad \omega\in\Theta, \tag{6c}$$

and

$$\boldsymbol{f}(x,y,t,\omega)\cdot\boldsymbol{n}(x,y)=\gamma(\omega)q(x,y,t), \qquad \forall(x,y)\in\Gamma_o,\quad t\in T,\quad \omega\in\Theta, \tag{7a}$$

$$\rho(x,y,0,\omega)=\rho^0(x,y), \qquad \forall(x,y)\in\Omega,\quad \omega\in\Theta, \tag{7b}$$

$$\phi(x,y,t,\omega)=0, \qquad \forall(x,y)\in\Gamma_d,\quad t\in T,\quad \omega\in\Theta, \tag{7c}$$

where $\gamma(\omega)$ is the scaling factor obtained from a certain distribution and ω is the random variable in the random space Θ. In this study, the demand is assumed to follow a lognormal distribution. The impact of demand stochasticity is reflected in the average traffic demand q being scaled by the factor $\gamma(\omega)$.

2.2.2. Problem B: Behavioral stochasticity

To incorporate behavioral stochasticity into the model, the original deterministic model for a single group of pedestrians is extended to include m sets of PDEs with different modeling parameters, where m is the number of pedestrian groups considered in this model. Each group of pedestrians has similar characteristics. In this study, the key parameter that describes the movement characteristics, i.e., the free-flow speed u_f, is treated as the stochastic input and classified into m intervals $I_i, i = 1, 2, \dots, m$. These speed intervals satisfy $I_i \cap I_j = \varnothing,\ \forall i \neq j$. If the free-flow speed is represented as a continuous distribution, the range can also be divided into m intervals. For the i-th group of pedestrians, the movement dynamics are described with a deterministic model that uses the middle value of the speed interval, $\bar{u}_{f,i}$. Without loss of generality, the speed intervals and their middle-value $\bar{u}_{f,i}$ for the i-th group of pedestrians are presented in ascending order, i.e., $\bar{u}_{f,1} < \bar{u}_{f,2} < \cdots < \bar{u}_{f,m-1} < \bar{u}_{f,m}$. Through this adjustment, the previous deterministic model is modified as

$$\frac{\partial}{\partial t}\rho_i(x,y,t)+\nabla\cdot\boldsymbol{f}_i(x,y,t)=0, \qquad \forall(x,y)\in\Omega,\quad t\in T,\quad i=1,2,\dots,m, \tag{8a}$$

$$C_i(\boldsymbol{\rho})\frac{\boldsymbol{f}_i(x,y,t)}{\|\boldsymbol{f}_i(x,y,t)\|}=-\nabla\phi_i(x,y,t), \qquad \forall(x,y)\in\Omega,\quad t\in T,\quad i=1,2,\dots,m, \tag{8b}$$

$$\left\|\nabla\phi_i(x,y,t)\right\|=C_i(\boldsymbol{\rho}), \qquad \forall(x,y)\in\Omega,\quad t\in T,\quad i=1,2,\dots,m, \tag{8c}$$

and

$$\boldsymbol{f}_i(x,y,t)\cdot\boldsymbol{n}(x,y)=q_i(x,y,t), \qquad \forall(x,y)\in\Gamma_o,\quad t\in T,\quad i=1,2,\dots,m, \tag{9a}$$

$$\rho_i(x,y,0)=\rho_i^0(x,y), \qquad \forall(x,y)\in\Omega,\quad i=1,2,\dots,m, \tag{9b}$$

$$\phi_i(x,y,t)=0, \qquad \forall(x,y)\in\Gamma_d,\quad t\in T,\quad i=1,2,\dots,m, \tag{9c}$$

where $\boldsymbol{\rho}=\{\rho_1,\rho_2,\dots,\rho_m\}$, subscript i represents the group class i, and the flow of the i-th pedestrian group satisfies $\|\boldsymbol{f}_i(x,y,t)\| = \rho_i(x,y,t)U_i(\boldsymbol{\rho})$. The speed of the i-th group of pedestrians is defined as

$$U_i(\boldsymbol{\rho})=\bar{u}_{f,i}\left\{1-\exp\left[\frac{C_0}{\bar{u}_{f,i}}\left(1-\frac{\rho_{\max}}{\tilde{\rho}}\right)\right]\right\}, \tag{10}$$

where $\tilde{\rho} = \sum_{i=1}^{m} \rho_i$ is the total density. Futhermore, the cost is defined as

$$C_i(\boldsymbol{\rho}) = \frac{1}{U_i(\boldsymbol{\rho})} + G(\boldsymbol{\rho}). \tag{11}$$

Here, the (estimated) travel time $1/U_i(\boldsymbol{\rho})$ and discomfort level $G(\boldsymbol{\rho})$ both depend on the local total density. Behavioral stochasticity is incorporated into the model by determining the inflow condition $q_i(x, y, t)$. The magnitude of the total inflow $q(x, y, t)$ is fixed (although it varies with time) but heterogeneous and may belong to different pedestrian groups. To describe this heterogeneity, the inflow boundary Γ_o and time duration T are divided into $d = d_p \times d_q$ space-time blocks, where d_p is the number of blocks for the inflow boundary, and d_q is the number of blocks for the time duration. Each interval can be denoted as

$$\mathbf{L}_l : \quad (x, y) \in \Gamma_{o,j_l} \text{ and } t \in T_{k_l}, \quad l = 1, 2, \dots, d, \tag{12}$$

where $1 \le j_l \le d_p$ and $1 \le k_l \le d_q$. In each block $\mathbf{L}_l$, the free-flow speed $u_{f,l}(\omega_l)$ is assumed to follow a probabilistic distribution and is assigned to a certain group of pedestrians according to its magnitude, i.e., $\forall (x, y, t) \in \mathbf{L}_l$, $i = 1, \dots, m$,

$$q_i(x, y, t) = \begin{cases} q(x, y, t), & \text{if} \quad u_{f,l}(\omega_l) \in I_i, \\ 0, & \text{otherwise.} \end{cases} \tag{13}$$

Here, ω_l represents the random variable in block $\mathbf{L}_l$. Notably, the number of dimensions for this stochastic problem is d, and the parameter in each interval follows an independent probabilistic distribution.

3. Computational schemes

This section describes the solution method for stochastic pedestrian models, which relies on repeated random sampling, i.e., the MC method. For each sample, as the inputs are all deterministic, the PDE set can be numerically solved using high-order computation schemes (Huang et al., 2009) such as the fifth-order weighted essentially non-oscillatory (WENO) scheme for the conservation law Eq. (1a), third-order fast sweeping method for the eikonal Eq. (1c), and third-order total-variation-diminishing (TVD) Runge-Kutta scheme for time discretization. The following sections introduce the numerical schemes and describe their integration with the MC or QMC method to capture the stochasticity.

3.1. Numerical schemes for solving partial differential equations

Assume that the domain is divided by fixed Cartesian meshes

$$x_{i+1} = x_i + \Delta x, \quad y_{j+1} = y_j + \Delta y, \tag{14}$$

where Δx and Δy are uniform mesh sizes in the x- and y-directions, respectively. $\rho_{i,j}$ and $\boldsymbol{f}_{i,j} = ((f_1)_{i,j}, (f_2)_{i,j})$ denote the approximations of ρ and $\boldsymbol{f}$, respectively, at grid point (x_i, y_j). The semi-discrete form of Eq. (1a) is

$$\frac{d}{dt}\rho_{i,j} = -\frac{1}{\Delta x}\left((\hat{f}_1)_{i+1/2,j} - (\hat{f}_1)_{i-1/2,j}\right) - \frac{1}{\Delta y}\left((\hat{f}_2)_{i,j+1/2} - (\hat{f}_2)_{i,j-1/2}\right). \tag{15}$$

The numerical fluxes $(\hat{f}_1)_{i+1/2,j}$ and $(\hat{f}_2)_{i,j+1/2}$ at the half-point are obtained by the one-dimensional fifth-order finite difference WENO scheme based on Lax-Friedrichs flux splitting (Jiang and Shu, 1996). After spatial discretization, the semi-discrete scheme is equivalent to a first-order ordinary differential equation system $\rho_t = L(\rho)$, where $L(\rho)$ is the spatial operator. Subsequently, the third-order TVD Runge-Kutta time integration (Shu and Osher, 1988), which is a convex combination of three Euler forward steps, is applied to evolve the solution:

$$\rho^{(1)} = \rho^n + \Delta t L(\rho^n), \tag{16a}$$

$$\rho^{(2)} = \frac{3}{4}\rho^n + \frac{1}{4}\left(\rho^{(1)} + \Delta t L(\rho^{(1)})\right), \tag{16b}$$

$$\rho^{n+1} = \frac{1}{3}\rho^n + \frac{2}{3}\left(\rho^{(2)} + \Delta t L(\rho^{(2)})\right), \tag{16c}$$

where Δt is the time step, and the superscript denotes the time level.

To obtain the flux $\boldsymbol{f}_{i,j}$ using Eq. (1b), the value of ϕ must be determined through Eq. (1c). The discretized form of the eikonal equation (1c) is

$$\hat{H}\left((\phi_x)^-_{i,j}, (\phi_x)^+_{i,j}; (\phi_y)^-_{i,j}, (\phi_y)^+_{i,j}\right) = c(x_i, y_j, t^n), \tag{17}$$

where $\hat{H}$ is the Godunov-type monotone Hamiltonian, and $(\phi_x)^{\pm}$ and $(\phi_y)^{\pm}$ are the WENO approximations of the left and right derivatives of ϕ in the x and y directions, respectively. The fast sweeping method with the third-order WENO scheme (Zhang et al., 2006) is applied to solve this equation. The boundary conditions are further explained in Section 4.

Given the density ρ^n at time level t_n, the following steps are implemented to obtain the density ρ^{n+1} through Euler forward time discretization:

1. Obtain the cost function c using Eq. (4);
2. Solve the eikonal Eq. (1c) using the fast sweeping method based on a third-order WENO discretization to obtain ϕ;

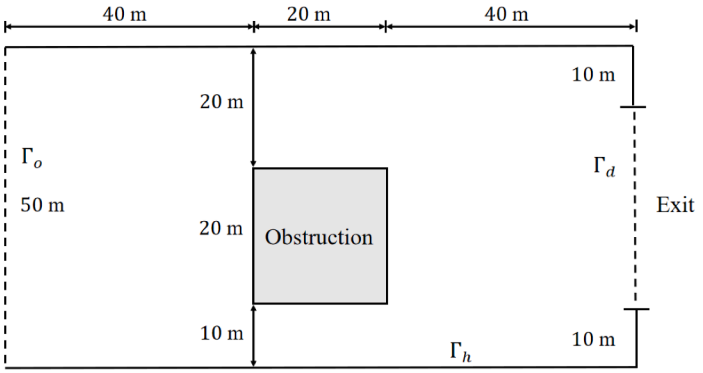

Fig. 2. Geometry of the railway platform.

3. Derive the magnitude $\|\boldsymbol{f}\|$ of flux $\boldsymbol{f}$ from Eqs. (2) and (3);
4. Use Eq. (1b) to determine the flux $\boldsymbol{f}$;
5. Apply the fifth-order Lax-Friedrichs WENO scheme to obtain ρ^{n+1} by solving the conservation Eq. (1a).

The third-order TVD Runge-Kutta time discretization is thus a convex combination of three Euler forward steps. This procedure is repeated until the end of the analysis period.

3.2. MC and QMC methods

In the algorithm for the deterministic model, the MC method can be applied to update the parameters and boundary conditions. In particular, the MC method uses random sampling and statistical modeling to estimate mathematical functions and simulate the operations of stochastic systems.

A complete MC procedure involves the following steps.

1. Sample random inputs $\{\boldsymbol{\omega}_n = (\omega_n^1, \omega_n^2, \dots, \omega_n^d)\}_{n=1}^N$ according to the specified distribution. Here, the integer d represents the number of dimensions in the stochastic problem.
2. Update the model with sampled inputs using Eqs. (6) or (8).
3. Solve the deterministic model using the high-order numerical schemes and obtain the solutions $\boldsymbol{\rho}(x, y, t, \boldsymbol{\omega}_n)$.
4. Repeat steps (1), (2), and (3) an adequate number of times and derive the solution set $\{\boldsymbol{\rho}(x, y, t, \boldsymbol{\omega}_n)\}_{n=1}^N$.

The MC method is robust but time-consuming, as its half-order convergence rate is $O(N^{-\frac{1}{2}})$. To enhance the computational efficiency, in this study the QMC method is used as an alternative. The QMC method can achieve first-order convergence depending on the number of dimensions in the stochastic problem. The error of the QMC method, E_N, has the following upper bound (Caflisch, 1998):

$$E_N \leq C_d (lnN)^d N^{-1}, \tag{18}$$

where the parameter C_d is problem dependent. The following QMC sequences (Caflisch, 1998) are used in this study:

1. **Van der Corput sequence** ($d = 1$):
   Expand n in base 2:

$$n = a_m a_{m-1} \cdots a_1 a_0; \quad \text{(in base 2)} \tag{19}$$

   Obtain ω_n in base 2:

$$\omega_n = 0.a_0 a_1 \cdots a_m. \quad \text{(in base 2)} \tag{20}$$

2. **Halton sequence** ($d > 1$):
   Expand n in base p_k (p_k is the k-th prime):

$$n = a^k_{m_k} a^k_{m_k - 1} \cdots a^k_1 a^k_0; \quad \text{(in base } p_k) \tag{21}$$

   Obtain ω_n^k in base p_k:

$$\omega_n^k = 0.a_0^k a_1^k \cdots a_{m_k}^k. \quad \text{(in base } p_k) \tag{22}$$

4. Numerical examples

Consider a railway platform with a length of 100 m and width of 50 m, as shown in Fig. 2. Pedestrians enter the platform from the left boundary and exit through the gate on the right boundary. An obstruction sized 20 m by 20 m is presented in the middle of the platform. The study time horizon T is 240 s. The time-varying demand at the entrance is expressed as

$$\forall y \in (0,50), \quad q(0,y,t) = \begin{cases} t/100 & 0 \le t < 60, \\ 1.2 - t/100 & 60 \le t < 120, \\ 0 & 120 \le t, \end{cases} \tag{23}$$

where the flow is expressed in ped/m/s. The flow increases linearly from zero to a peak at $t = 60$ s, and then decreases linearly back to zero at $t = 120$ s. No pedestrian crosses the entrance after $t = 120$ s. The discomfort function is set as $G(\rho) = 0.002\rho^2$ for Problem A and $G(\boldsymbol{\rho}) = 0.002\tilde{\rho}^2$ for Problem B. The common parameters in the two stochastic problems, including the maximum density $\rho_{\max}$ and parameter C_0 in Eq. (3), are set as 6 ped/m^2 and 0.4, respectively.

The rectangular domain $[0,100] \times [0,50]$ (units: m) is discretized into a uniform grid of 100×50 points for the numerical simulations. The high-order finite difference scheme requires appropriate implementation of boundary conditions, which are given as follows:

1. At the inlet Γ_o, the flux $\boldsymbol{f}$ is determined using the sampled inflow, as described in Section 2.2. The values of ρ and ϕ at the points can be obtained through extrapolation using their values at the interior points.
2. On the walls Γ_h, the values at ghost points are set as $\boldsymbol{f} = 0$, $\rho = 0$ and $\phi = 10^{12}$.
3. At the outlet Γ_d, $\phi = 0$. The values of ρ and $\boldsymbol{f}$ at the ghost points are obtained through extrapolation from the interior point values.

To maintain numerical stability and accuracy, the maximum time step of evolution is restricted. For the fifth-order WENO and third-order TVD Runge-Kutta scheme (Gottlieb and Shu, 1998) in two dimensions, the time step is set as

$$\Delta t = \mathrm{CFL} \Big/ \left(\left(\frac{\alpha}{\Delta x} \right)^{\frac{5}{3}} + \left(\frac{\beta}{\Delta y} \right)^{\frac{5}{3}} \right), \tag{24}$$

where the coefficient $\mathrm{CFL} = 0.5$, $\alpha = \max_{i,j} |u|$, and $\beta = \max_{i,j} |v|$.

Finally, to investigate the convergence rate of the MC or QMC process, the global relative root mean square error between successive cases is considered:

$$E_\rho = \frac{\sqrt{\frac{1}{N_g} \sum_{i,j,k} (\rho_{i,j,k}^{(ref)} - \rho_{i,j,k}^{(N)})^2}}{\frac{1}{N_g} \sum_{i,j,k} \rho_{i,j,k}^{(ref)}} \times 100\%, \tag{25a}$$

$$E_\sigma = \frac{\sqrt{\frac{1}{N_g} \sum_{i,j,k} (\sigma_{i,j,k}^{(ref)} - \sigma_{i,j,k}^{(N)})^2}}{\frac{1}{N_g} \sum_{i,j,k} \sigma_{i,j,k}^{(ref)}} \times 100\%, \tag{25b}$$

where subscript k represents the integer time points satisfying $t_k = k \cdot \frac{T}{240}$, $k = 1, 2, \ldots, 240$. $\rho_{i,j,k}^{(N)}$ and $\sigma_{i,j,k}^{(N)}$ are the mean and standard deviation of the density for the grid point (x_i, y_j, t_k) in the case involving N incidents, respectively. $\rho_{i,j,k}^{(ref)}$ and $\sigma_{i,j,k}^{(ref)}$ are the reference solutions obtained from the MC results from a large number of samples (10,000 in this study), and N_g is the total number of space-time grid points.

4.1. Problem A: Demand stochasticity

In modeling day-to-day stochasticity, the varying traffic demand is assumed to follow a probabilistic distribution. Therefore, the inflow boundary condition is set as

$$f_1(0,y,t) = \gamma(\omega) q(0,y,t), \tag{26}$$

where $\gamma(\omega)$ is the scaling factor obtained from the lognormal distribution with a mean of 1.0 and a standard deviation of either 0.1 or 0.2. In modeling within-day stochasticity, the scaling factor $\gamma(\omega)$ follows the same distribution as that in the day-to-day case but varies every ten seconds within the first 120 s.

Fig. 3 shows the contours of the mean density distribution at space-time point (x, y) in the day-to-day stochastic process (SD = 0.1) at $30, 60, \ldots, 210, 240$ s. These contours show the movement pattern of pedestrians, which are similar to those obtained using the deterministic model proposed by Huang et al. (2009). Two shocks can be observed before the square obstacle (maximum density of 1.38 ped/m^2) at $t = 90$ s. Furthermore, due to the capacity drop resulting from the obstacle between $x \in [40, 60]$ m, the mean density in the surrounding region is higher than that in the free area. Similar shocks are also observed near the corners of the exit, resulting in the formation of another bottleneck. These findings highlight that the dynamics of the first moment, i.e., the mean density, can reproduce the congestion in obstructed walking facilities.

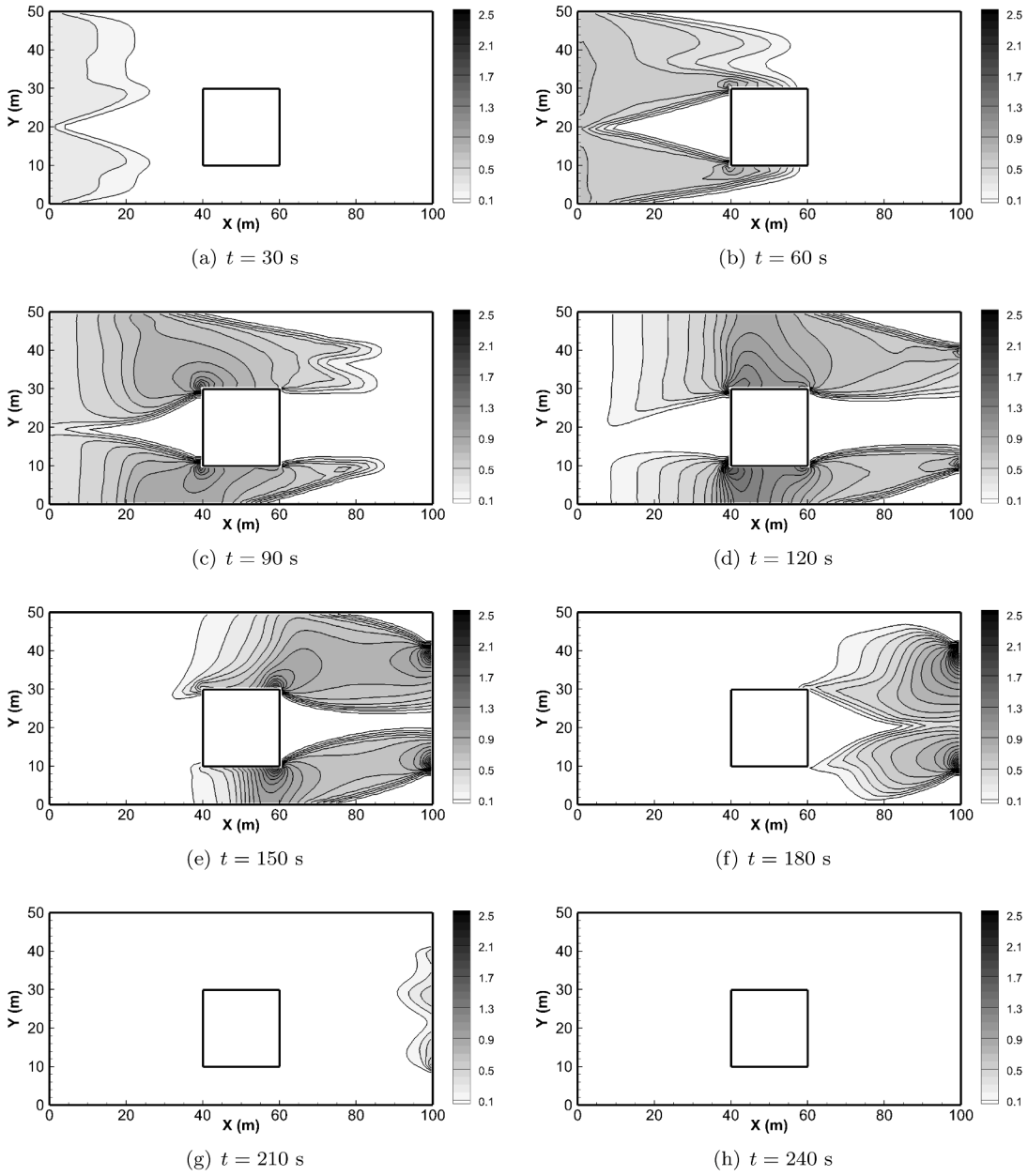

Fig. 3. Day-to-day (SD = 0.1): Contours of the mean density at different times (26 contours from 0 to 2.5).

Fig. 4 shows the contours of the standard deviation of the density distribution at space-time point (x, y) in the day-to-day stochastic process (SD = 0.1) at $30, 60, \ldots, 210, 240$ s. Two types of shocks can be observed: The first shock occurs at the edge of the moving pedestrians, such as the edge at $x \in [0, 40]$ m, $y \in [20, 30]$ m and $t = 90$ s. The increased SD is attributable to the route strategy of pedestrians. More pedestrians tend to move along the edge of the flock, while the maximum density within the flock does not increase significantly even with increased demand. The second shock is observed when pedestrians encounter a bottleneck, for example, at $t = 120, 150, 210$ s. This shock results from the physical constraints imposed on pedestrian flow with stochastic demand. Notably, the peak position of this SD shock always occurs behind that of the mean density along the direction of movement. This phenomenon indicates that as pedestrians enter the walking facility, the density in the congested flock is homogenized because of the increased demand, resulting in a larger variation behind the peak position of the mean density. The information provided by the second moment, i.e., the SD of the density distribution, can help identify areas with a large variance in density and facilitate the formulation of adaptive control strategies to enhance the level of service in walking environments.

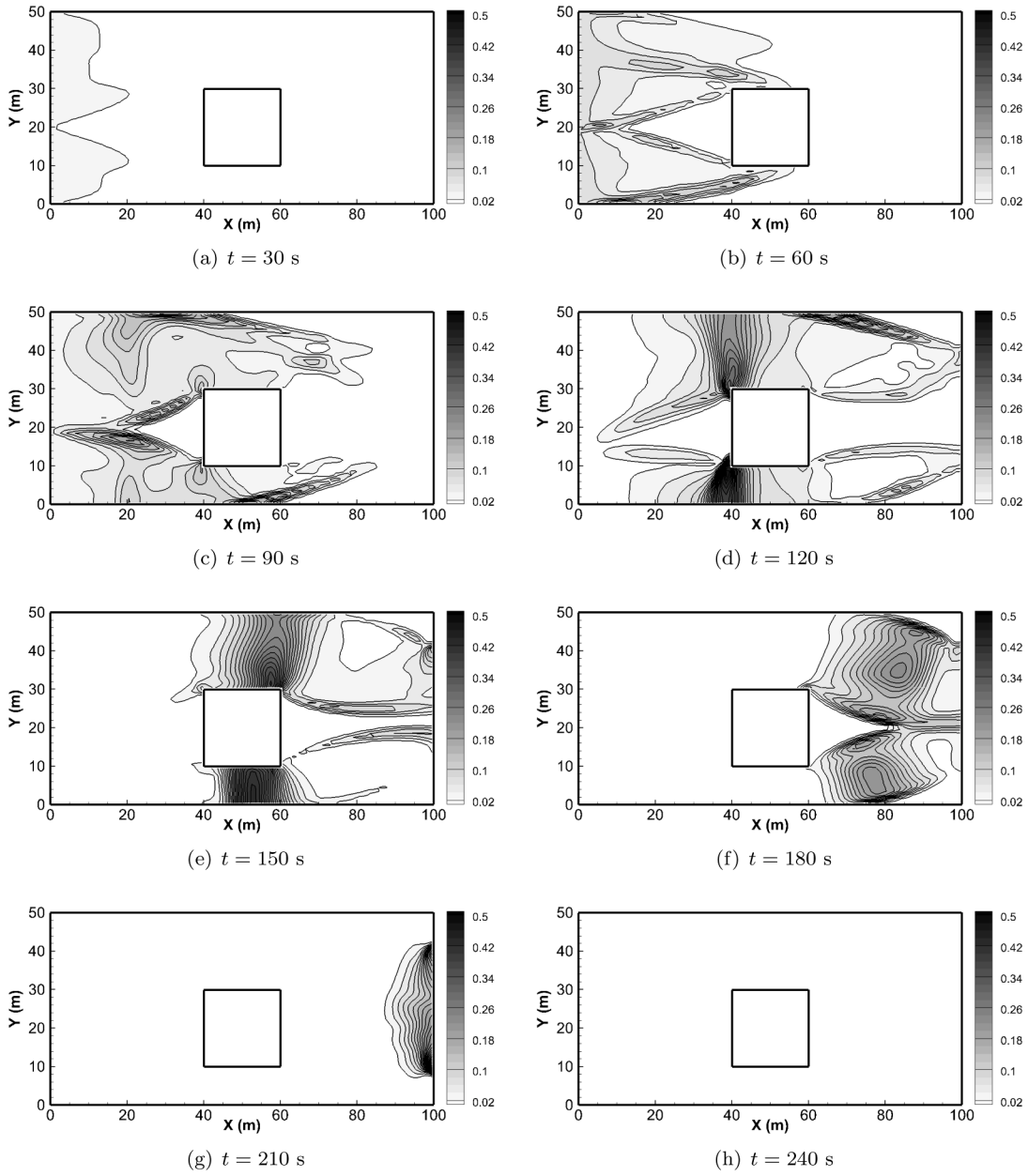

Fig. 4. Day-to-day (SD = 0.1): Contours of the standard deviation of density at different times (26 contours from 0 to 0.5).

To further illustrate the difference in density distributions under stochastic demand, Figs. 5 and 6 plot the pedestrian density at section $y = 9.5$ m. For comparison, the simulation results obtained from the deterministic model using the averaged demand, Eq. (23), are also plotted and labeled "mean demand". In the case of day-to-day stochasticity, the mean density distribution derived from the stochastic process (labeled "mean density") is considerably different from that obtained using the deterministic model. This difference is attributable to the nonlinearity of the simulation process and is intensified as the standard deviation increases. Moreover, the solutions obtained from the stochastic model produce a density range within the 95% confidence interval, enabling the evaluation of the robustness of the walking facility.

Similar results are observed in the within-day stochastic case, although the difference in mean densities obtained using the stochastic model and deterministic model is less significant. This comparison demonstrates that the day-to-day stochasticity more notably affects the density variance than the within-day stochasticity at the same level of randomness.

Figs. 7 and 8 show the convergence rates in each case with SD = 0.1. The ground truth solution is obtained through the MC process with $10,000$ independent simulations. The convergence of the QMC is compared with that of the MC method, and the results

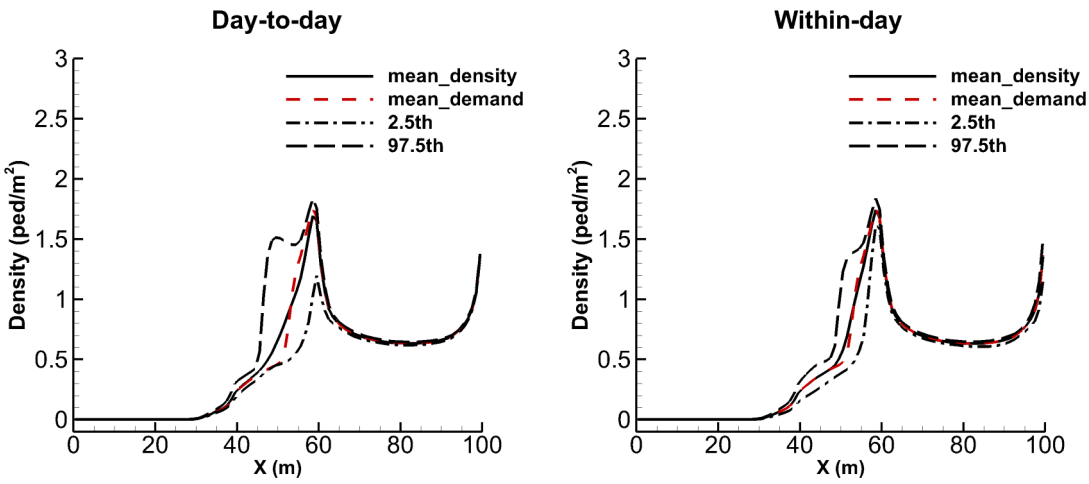

(a) Day-to-day case (b) Within-day case

Fig. 5. Pedestrian density at section $y = 9.5$ m at $t = 150$ s (SD = 0.1).

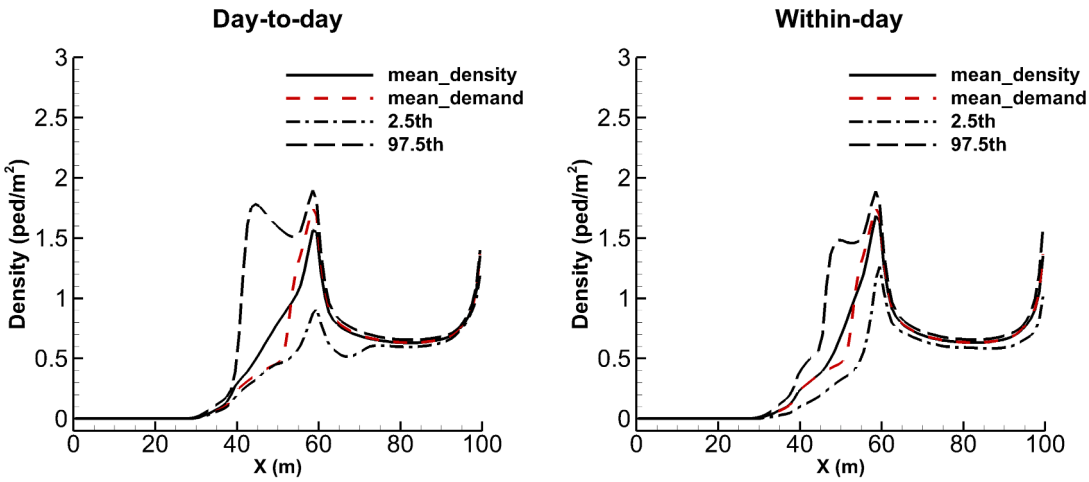

(a) Day-to-day case (b) Within-day case

Fig. 6. Pedestrian density at section $y = 9.5$ m at $t = 150$ s (SD = 0.2).

Table 1
Comparison of the convergence orders of the MC and QMC methods.

Case	Dimension	E_ρ-MC	E_σ-MC	E_ρ-QMC	E_σ-QMC
Day-to-day	1	0.39	0.42	0.93	0.77
Within-day	12	0.31	0.55	0.33	0.23

indicate that the QMC outperforms the MC method in the day-to-day stochastic case. Table 1 lists the dimensions and convergence orders for the two methods in the two cases. The QMC is more efficient than the MC method for low-dimensional stochastic problems but less efficient when the dimension of the random variables is high. This outcome can be attributed to the term $(lnN)^d$ in Eq. (18), which relies on the dimension of the stochastic problem and considerably affects the efficiency.

4.2. Problem B: Behavioral stochasticity

Problem B focuses on the behavioral stochasticity by introducing random movement characteristics of the free-flow speed in the fundamental diagram. In this study, $m = 20$, and the speed intervals, $I_i, i = 1, 2, \ldots, 20$, are defined as $(0, 0.1]$,$(0.1, 0.2]$,…,$(1.9, 2.0]$

Table 2
Blocks and corresponding dimensions.

Block	$L_b \times T_b$	Dimension $d_p \times d_q = d$
1	5 m × 5 s	$10 \times 24 = 240$
2	10 m × 10 s	$5 \times 12 = 60$
3	25 m × 20 s	$2 \times 6 = 12$

Table 3
Comparison of the convergence orders of the MC and QMC methods.

Case	Dimension	E_ρ-MC	E_σ-MC	E_ρ-QMC	E_σ-QMC
Block 5 m × 5 s	240	0.50	0.48	0.05	0.01
Block 10 m × 10 s	60	0.44	0.49	0.32	0.04
Block 25 m × 20 s	12	0.50	0.49	0.40	0.49

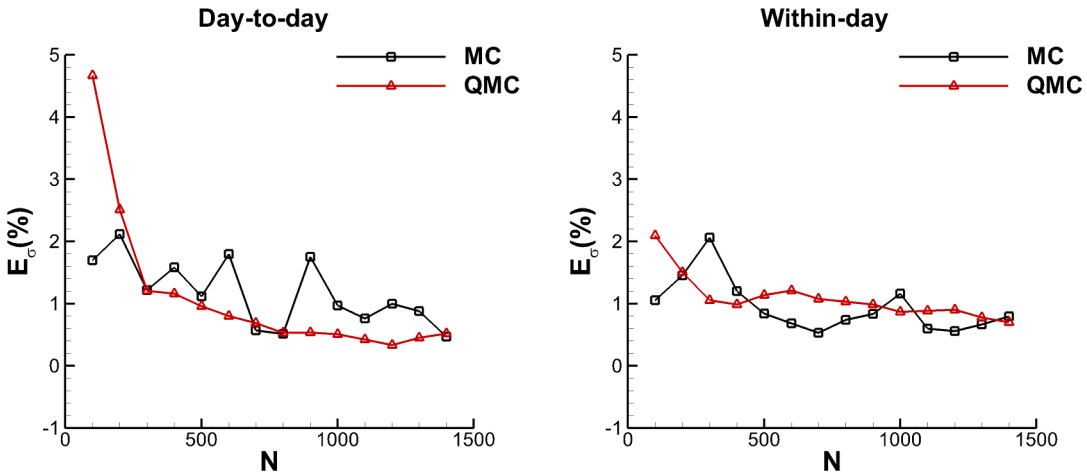

Fig. 7. Overall error and convergence of the mean density in different cases.

m/s, respectively. Thus, the parameters of free-flow speed in Eq. (8) are assigned the midpoint values of these intervals, i.e., $\bar{u}_{f,1} = 0.05, \bar{u}_{f,2} = 0.15, \ldots, \bar{u}_{f,20} = 1.95$.

According to Eq. (12), the inflow boundary Γ_o ($x = 0$ m, $y \in [0, 50]$ m) and time duration T ($t \in [0, 120]$ s) are divided into blocks of different sizes for each case, as shown in Table 2. In the first case, the block size is 5 m × 5 s. Thus, $10 \times 12 = 240$ random inputs of the free-flow speed $u_{f,l}(\omega_l)$ are generated, which indicates that the dimension of this stochastic problem is 240. Similarly, the second and third cases involve 60 and 12 random inputs, respectively. The free-flow speed $u_{f,l}(\omega_l)$ is assumed to follow the lognormal distribution (mean = 1.0 and SD = 0.1). Fig. 9 shows the pedestrian density at section $y = 9.5$ m. As in the case of Problem A, the simulation results of the stochastic model are considerably different from those of the deterministic model, and the density range is within the 95% confidence interval, which demonstrates the applicability of the model. The comparison of cases with different dimensions shows that larger dimensions of stochastic settings correspond to a reduced difference in the results of the two models and the density distributions in the MC simulations. These trends can be explained by the fact that increasing the blocks at the inflow boundary decreases the heterogeneity among the integrated inflow. For example, the heterogeneity of the random inputs of the MC process in the third case, in which the number of variables is $2 \times 6 = 12$, is more notable than that in the first case, in which the number of variables is $10 \times 24 = 240$.

Figs. 10 and 11 compare the performance of the MC and QMC methods. The ground truth solution is obtained through the MC process using $10,000$ independent simulations. In the case with 240 random variables, the error associated with the QMC does not converge before $N = 800$. In comparison, in the case with 60 random variables, the convergence rate is higher, and the errors E_ρ and E_σ decrease to approximately 5% and 22%, respectively. In the case with 12 random variables, the convergence rate of QMC is similar to that of the MC method. Table 3 summarizes the dimension and convergence order for each case. The values indicate that the convergence rate of the MC method is half-order, consistent with the observation in Problem A that the dimension of the stochastic problem considerably influences the convergence order of the QMC. Therefore, for most cases involving behavioral stochasticity, the MC method outperforms the QMC.

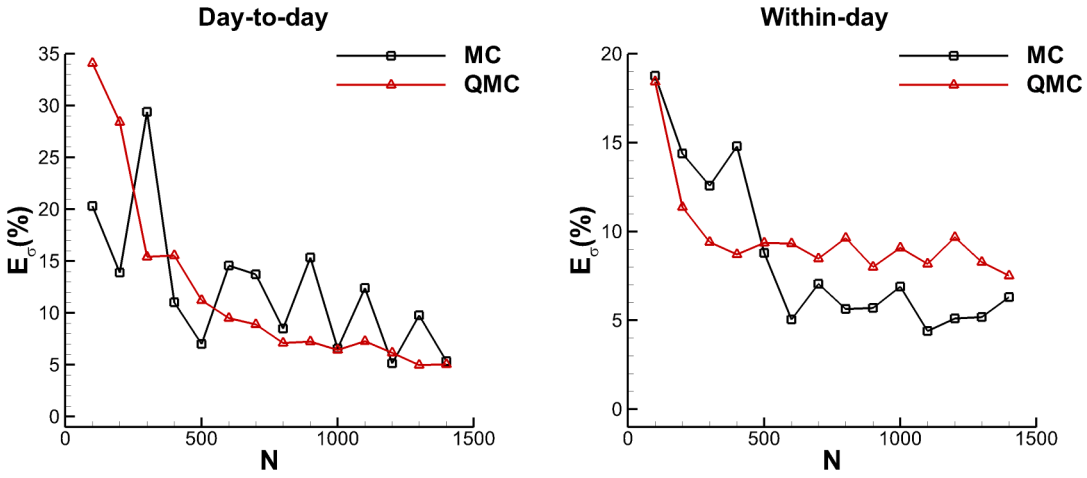

Fig. 8. Overall error and convergence of the standard deviation of density in different cases.

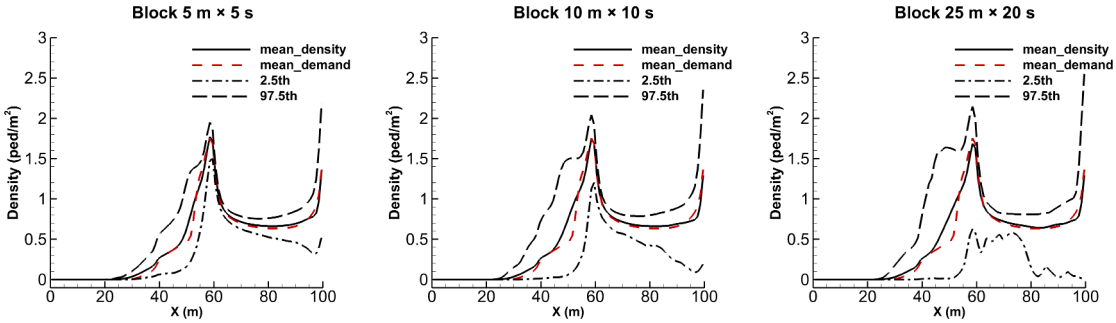

Fig. 9. Block 5 m × 5 s, 10 m × 10 s, 25 m × 20 s: The pedestrian density at section $y = 9.5$ m at $t = 150$ s.

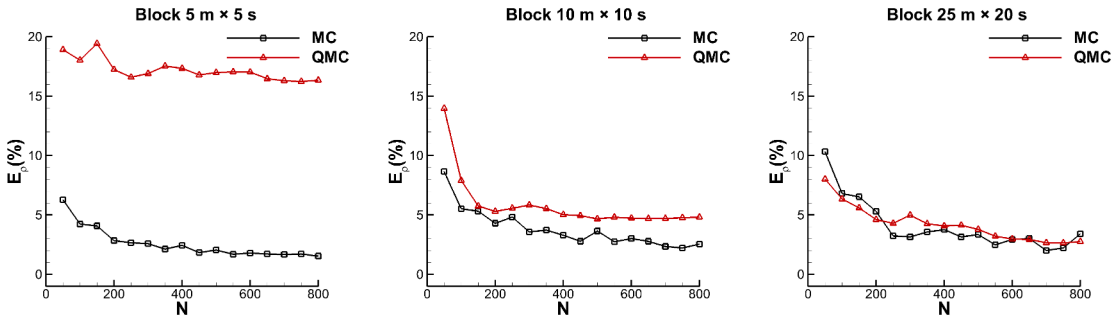

Fig. 10. Overall error and convergence of the mean density in different cases.

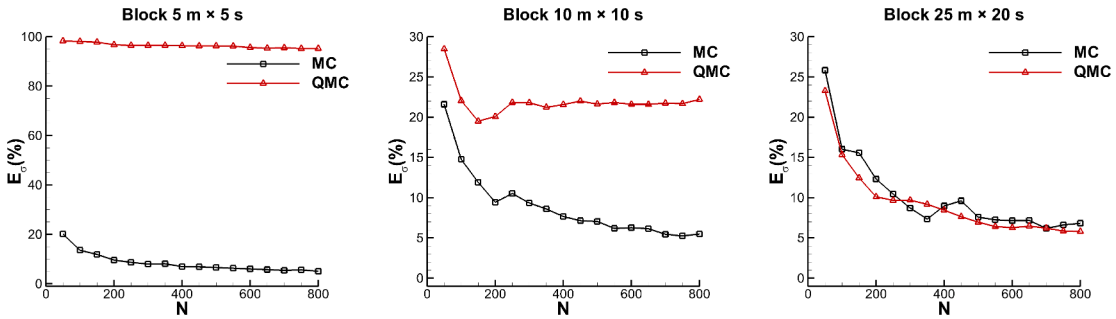

Fig. 11. Overall error and convergence of the standard deviation of density in different cases.

5. Conclusion

A dynamic continuum approach for modeling stochastic pedestrian dynamics is developed in this paper. The original deterministic first-order continuum model for pedestrian flow is extended to incorporate two types of stochastic problems: demand stochasticity and behavioral stochasticity. Demand stochasticity focuses on mathematically describing the traffic demand at the inflow boundary, considering the random inflow magnitudes along both the day-to-day and within-day dimensions. Behavioral stochasticity accounts for the heterogeneity of entering pedestrians, classified based on a specific parameter in the pedestrian flow dynamics, across distinct spatial and temporal blocks. The proposed stochastic problems, formulated as PDE systems with stochastic inputs, are solved using a combination of MC or QMC methods and high-order numerical schemes. The numerical schemes include the fifth-order WENO approach and fast sweeping method for discretizing the conservation equation and eikonal equation, respectively.

The proposed method is applied to numerical simulations on a two-dimensional platform, and the convergence of results obtained from the MC and QMC methods validates their effectiveness. A comparison of the convergence rates of the two sampling methods reveals that the QMC method outperforms the MC method in low-dimensional stochastic problems. In terms of practical applications, the numerical results not only provide insights into the average density distribution but also yield the density range within a 95% confidence interval. This information can help evaluate the robustness of walking facilities. Furthermore, the simulations demonstrate that the average density derived from the stochastic model significantly differs from that obtained using the deterministic model, highlighting the importance of incorporating stochasticity in practical applications. This difference depends on the randomness of input levels and number of stochastic dimensions.

Notably, both the MC and QMC methods are time consuming, although QMC exhibits certain advantages in solving low-dimensional stochastic problems. Future work could focus on developing more efficient numerical methods for stochastic models, such as the polynomial chaos expansion method (Xiu and Karniadakis, 2002), dynamically bi-orthogonal method (Cheng et al., 2013) and multi-element probabilistic collocation method (Liu et al., 2025). In addition to enhancing the solution efficiency, it is necessary to calibrate the probabilistic distribution of stochastic inputs based on real-life data. This calibration is expected to enhance the practicability of the proposed models and solution methods, ensuring their applicability to real-world scenarios.

Acknowledgement

The work described in this paper was supported by grants from the Research Grants Council of the Hong Kong Special Administrative Region, China (Project Nos. 17204919, 17202824). The second author was supported by grants from the National Natural Science Foundation of China (Grant No. 52302378) and the Shanghai Super Postdoctoral Incentive Program, the third author was supported by the Francis S Y Bong Professorship in Engineering, the fourth author was supported by NSF grant DMS-2309249.

References

Barreiro-Gomez, J., Masmoudi, N., 2023. Differential games for crowd dynamics and applications. Math. Models Methods Appl. Sci. 33 (13), 2703–2742.
Bouadi, M., Jia, B., Jiang, R., Li, X., Gao, Z.Y., 2022. Stability analysis of stochastic second-order macroscopic continuum models and numerical simulations. Transp. Res. Part B 164, 193–209.
Brilon, W., Geistefeldt, J., Regler, M., 2005. Reliability of freeway traffic flow: a stochastic concept of capacity. In: Proceedings of the 16th International Symposium on Transportation and Traffic Theory. Vol. 125143. Citeseer.
Burger, M., Di Francesco, M., Markowich, P.A., Wolfram, M.-T., 2013. On a mean field game optimal control approach modeling fast exit scenarios in human crowds. In: 52nd IEEE Conference on Decision and Control. IEEE, pp. 3128–3133.
Caflisch, R.E., 1998. Monte carlo and quasi-monte carlo methods. Acta Numer. 7, 1–49.
Cao, K., Chen, Y., Stuart, D., Yue, D., 2015. Cyber-physical modeling and control of crowd of pedestrians: a review and new framework. IEEE/CAA J. Autom. Sin. 2 (3), 334–344.
Cheng, M., Hou, T.Y., Zhang, Z., 2013. A dynamically bi-orthogonal method for time-dependent stochastic partial differential equations I: Derivation and algorithms. J. Comput. Phys. 242, 843–868.
Djehiche, B., Tcheukam, A., Tembine, H., 2017. A mean-field game of evacuation in multilevel building. IEEE Trans. Automat. Contr. 62 (10), 5154–5169.
Dogbé, C., 2010. Modeling crowd dynamics by the mean-field limit approach. Math. Comput. Model. 52 (9–10), 1506–1520.
Ezzati Amini, R., Katrakazas, C., Antoniou, C., 2019. Negotiation and decision-making for a pedestrian roadway crossing: A literature review. Sustainability 11 (23), 6713.
Fan, T., Wong, S.C., Zhang, Z., Du, J., 2023. A dynamically bi-orthogonal solution method for a stochastic Lighthill-Whitham-Richards traffic flow model. Comput.-Aided Civ. Infrastruct. Eng. 38 (11), 1447–1461.
Fan, T., Wong, S.C., Zhang, Z., Du, J., 2024. Stochastic Lighthill-Whitham-Richards traffic flow model for nonlinear speed-density relationships. Transportmetrica B: Transport Dyn. 12 (1), 2419402.
Ghattassi, M., Masmoudi, N., 2025. Non-separable mean field games for pedestrian flow: Generalized hughes model. Math. Models Methods Appl. Sci. 35 (07), 1571–1607.
Gottlieb, S., Shu, C.W., 1998. Total variation diminishing Runge-Kutta schemes. Math. Comput. 67 (221), 73–85.
Huang, L., Wong, S.C., Zhang, M., Shu, C., Lam, W.H.K., 2009. Revisiting Hughes' dynamic continuum model for pedestrian flow and the development of an efficient solution algorithm. Transp. Res. Part B 43 (1), 127–141.
Hughes, R.L., 2002. A continuum theory for the flow of pedestrians. Transp. Res. Part B 36 (6), 507–535.
Hänseler, F.S., Molyneaux, N.A., Bierlaire, M., 2017. Estimation of pedestrian origin-destination demand in train stations. Transp. Sci. 51 (3), 981–997.
Jabari, S.E., Zheng, J., Liu, H.X., 2014. A probabilistic stationary speed-density relation based on Newell's simplified car-following model. Transp. Res. Part B 68, 205–223.
Jiang, G.S., Shu, C.W., 1996. Efficient implementation of weighted ENO schemes. J. Comput. Phys. 126 (1), 202–228.
Jiang, Y.Q., Wong, S.C., Ho, H.W., Zhang, P., Liu, R.X., Sumalee, A., 2011. A dynamic traffic assignment model for a continuum transportation system. Transp. Res. Part B 45, 343–363.
Jiang, Y.Q., Zhang, P., Wong, S.C., Liu, R.X., 2010. A higher-order macroscopic model for pedestrian flows. Physica A 389 (21), 4623–4635.
Kerner, B.S., Klenov, S.L., 2006. Probabilistic breakdown phenomenon at on-ramp bottlenecks in three-phase traffic theory: congestion nucleation in spatially non-homogeneous traffic. Physica A 364, 473–492.

Kesting, A., Treiber, M., Helbing, D., 2010. Enhanced intelligent driver model to access the impact of driving strategies on traffic capacity. Phil. Trans. R. Soc. A Math. Phys. Eng. Sci. 368 (1928), 4585–4605.
Lachapelle, A., Wolfram, M.-T., 2011. On a mean field game approach modeling congestion and aversion in pedestrian crowds. Transp. Res. Part B 45 (10), 1572–1589.
Li, J., Chen, Q.Y., Wang, H., Ni, D., 2012. Analysis of LWR model with fundamental diagram subject to uncertainties. Transportmetrica 8 (6), 387–405.
Liang, H., Du, J., Wong, S.C., 2021. A continuum model for pedestrian flow with explicit consideration of crowd force and panic effects. Transp. Res. Part B 149, 100–117.
Liu, Z., Wong, S.C., Yang, L., Shu, C.-W., Zhang, M., 2025. Multi-element probabilistic collocation solution for dynamic continuum pedestrian models with random inputs. Transp. Res. Part C 174, 105104.
Newell, G.F., 1961. Nonlinear effects in the dynamics of car following. Oper. Res. 9 (2), 209–229.
Ngoduy, D., 2021. Noise-induced instability of a class of stochastic higher order continuum traffic models. Transp. Res. Part B 150, 260–278.
Parisi, D.R., Sartorio, A.G., Colonnello, J.R., Garcimartín, A., Pugnaloni, L.A., Zuriguel, I., 2021. Pedestrian dynamics at the running of the bulls evidence an inaccessible region in the fundamental diagram. Proc. Natl. Acad. Sci. 118 (50), 1–9.
Parry, K., Hazelton, M.L., 2013. Bayesian inference for day-to-day dynamic traffic models. Transp. Res. Part B 50, 104–115.
Ramírez, M., Torres, F., Toledo, B.A., Coello, M., Correa-Burrows, P., Rogan, J., Valdivia, J.A., 2019. Unpredictability in pedestrian flow: the impact of stochasticity and anxiety in the event of an emergency. Physica A 531, 121742.
Sayegh, A.S., Connors, R.D., Tate, J.E., 2018. Uncertainty propagation from the cell transmission traffic flow model to emission predictions: a data-driven approach. Transp. Sci. 52 (6), 1327–1346.
Shu, C.W., Osher, S., 1988. Efficient implementation of essentially non-oscillatory shock-capturing schemes. J. Comput. Phys. 77 (2), 439–471.
Sumalee, A., Uchida, K., Lam, W.H.K., 2011a. Stochastic multi-modal transport network under demand uncertainties and adverse weather condition. Transp. Res. Part C 19 (2), 338–350.
Sumalee, A., Zhong, R.X., Pan, T.L., Szeto, W.Y., 2011b. Stochastic cell transmission model (SCTM): A stochastic dynamic traffic model for traffic state surveillance and assignment. Transp. Res. Part B 45 (3), 507–533.
Tordeux, A., Schadschneider, A., 2016. White and relaxed noises in optimal velocity models for pedestrian flow with stop-and-go waves. J. Phys. A: Math. Theor. 49 (18), 185101.
Wong, S.C., Leung, W.L., Chan, S.H., Lam, W.H.K., Yung, N.H.C., Liu, C.Y., Zhang, P., 2010. Bidirectional pedestrian stream model with oblique intersecting angle. J. Transp. Eng. 136 (3), 234–242.
Xiu, D., Karniadakis, G.E., 2002. The Wiener–Askey polynomial chaos for stochastic differential equations. SIAM J. Sci. Comput. 24 (2), 619–644.
Yuan, Y., Goñi-Ros, B., Bui, H., Daamen, W., Vu, H., Hoogendoorn, S.P., 2020. Macroscopic pedestrian flow simulation using smoothed particle hydrodynamics (SPH). Transp. Res. Part C 111, 334–351.
Zhang, Y.T., Zhao, H.K., Qian, J.L., 2006. High order fast sweeping methods for static Hamilton-Jacobi equations. J. Sci. Comput. 29 (1), 25–56.
Zhong, R.X., Sumalee, A., Pan, T.L., Lam, W.H.K., 2013. Stochastic cell transmission model for traffic network with demand and supply uncertainties. Transportmetrica A: Transport Sci. 9 (7), 567–602.